Middle East respiratory syndrome coronavirus vaccine based on a propagation-defective RNA replicon elicited sterilizing immunity in mice

J. Gutiérrez-Álvarez[a], J. M. Honrubia[a], A. Sanz-Bravo[a], E. González-Miranda[a], R. Fernández-Delgado[a], M. T. Rejas[b], S. Zúñiga[a], I. Sola[a], and L. Enjuanes[a,1]

[a]Department of Molecular and Cell Biology, Centro Nacional de Biotecnología (CNB-CSIC), Universidad Autónoma de Madrid 28049 Madrid, Spain; and [b]Electron Microscopy Service, Centro de Biología Molecular "Severo Ochoa" (CBMSO-CSIC-UAM), Universidad Autónoma de Madrid, Madrid 28049, Spain

Contributed by L. Enjuanes, September 2, 2021 (sent for review July 5, 2021; reviewed by Lisa E. Gralinski and Shinji Makino)

Self-amplifying RNA replicons are promising platforms for vaccine generation. Their defects in one or more essential functions for viral replication, particle assembly, or dissemination make them highly safe as vaccines. We previously showed that the deletion of the envelope (E) gene from the Middle East respiratory syndrome coronavirus (MERS-CoV) produces a replication-competent propagation-defective RNA replicon (MERS-CoV-ΔE). Evaluation of this replicon in mice expressing human dipeptidyl peptidase 4, the virus receptor, showed that the single deletion of the E gene generated an attenuated mutant. The combined deletion of the E gene with accessory open reading frames (ORFs) 3, 4a, 4b, and 5 resulted in a highly attenuated propagation-defective RNA replicon (MERS-CoV-Δ[3,4a,4b,5,E]). This RNA replicon induced sterilizing immunity in mice after challenge with a lethal dose of a virulent MERS-CoV, as no histopathological damage or infectious virus was detected in the lungs of challenged mice. The four mutants lacking the E gene were genetically stable, did not recombine with the E gene provided in trans during their passage in cell culture, and showed a propagation-defective phenotype in vivo. In addition, immunization with MERS-CoV-Δ[3,4a,4b,5,E] induced significant levels of neutralizing antibodies, indicating that MERS-CoV RNA replicons are highly safe and promising vaccine candidates.

coronavirus | MERS-CoV | vaccine | RNA replicon

Coronaviruses (CoVs) are a family of enveloped, positive-strand RNA viruses of the *Nidovirales* order. Specifically, the *Orthocoronavirinae* subfamily is divided into the *Alpha*, *Beta*, *Gamma*, and *Delta* genera (1–3). Viruses of these four genera can infect a wide range of birds and mammals, including humans (4–7), producing different clinical signs depending on the targeted tissue and organ (5, 8–10). Seven coronaviruses infecting humans (HCoVs) have been identified. Of them, HCoV-229E, HCoV-OC43, HCoV-NL63, and HCoV-HUK1 cause a common cold that is rarely complicated (5, 11). In contrast, severe acute respiratory syndrome coronavirus (SARS-CoV) (12, 13), Middle East respiratory syndrome coronavirus (MERS-CoV) (2, 14), and severe acute respiratory syndrome coronavirus 2 (SARS-CoV-2) (15, 16) cause a severe respiratory infection that can be fatal. Since the appearance of SARS-CoV, the investigation of CoVs has gained great relevance, especially considering that these three highly pathogenic HCoVs have emerged in the human population through zoonosis in the last 20 y: SARS-CoV in 2002 (12, 13) (number of cases: 8,437, average mortality: 10%; ref. 17), MERS-CoV in 2012 (2, 14) (2,589 cases and a mortality of 35% as of April 2021; ref. 18), and SARS-CoV-2 (146 million cases, 3.0 million deaths, April 2021; ref. 19) (15, 16).

Although different strategies to protect against MERS-CoV have been developed (20, 21), no vaccines or treatments for MERS-CoV have been approved for human use. Nonetheless, at least four vaccines have been developed at present (three based on viral vectors and one on DNA) (22–27), and one monoclonal antibody (28) is being tested in clinical trials. Generally, vaccine candidates have been based on the Spike (S) protein since this protein is the major target of virus-neutralizing antibodies (29), and it is responsible for binding to the cell receptor, dipeptidyl peptidase 4 (DPP4) (30). Among the S-based MERS-CoV vaccine candidates, subunit, DNA, and viral vector vaccines have been developed. However, there are certain specific limitations to each of these vaccine types. Subunit vaccines frequently require more than one dose to elicit efficient immunity, which in general, is not long lasting (20), and require an adjuvant to enhance the immune response or to induce mucosal immunity (31, 32). DNA vaccines generally induce weak responses in large animals and humans (33–36), although SARS-CoV-2 messenger RNA (mRNA) vaccines have shown excellent efficacy in humans (37, 38) and have been authorized for use in the COVID-19 pandemic (39, 40). The main limitation of viral vector vaccines is that a preexisting or newly generated response against the vector may decrease the effectiveness of the vaccine (41–43).

Significance

Coronaviruses (CoVs) have the largest genome among RNA viruses and a proofreading exoribonuclease (nsp14) responsible for high-fidelity RNA synthesis. These properties make CoVs very attractive for the establishment of vaccine platforms or viral vectors since they can stably store large amounts of information without genome integration. Using Middle East respiratory syndrome coronavirus (MERS-CoV) as a model, a propagation-deficient RNA replicon was generated by removing the envelope (E) gene (essential for viral morphogenesis and involved in virulence) and accessory genes 3, 4a, 4b, and 5 (responsible for antagonism of the innate immune response): MERS-CoV-Δ[3,4a,4b,5,E]. This replicon is strongly attenuated and elicits sterilizing protection after a single immunization, making it a promising vaccine candidate and an interesting platform for vector-based vaccine development.

Author contributions: J.G.-A., J.M.H., A.S.-B., E.G.-M., R.F.-D., M.T.R., and L.E. designed research; J.G.-A., J.M.H., A.S.-B., E.G.-M., R.F.-D., and M.T.R. performed research; J.G.-A. contributed new reagents/analytic tools; J.G.-A. analyzed data; I.S. and L.E. provided supervision; and J.G.-A., J.M.H., A.S.-B., E.G.-M., R.F.-D., S.Z., I.S., and L.E. wrote the paper.

Reviewers: L.E.G., The University of North Carolina at Chapel Hill; and S.M., The University of Texas Medical Branch.

Competing interest statement: The authors declare patent applications (pending) filed by their institution.

[1]To whom correspondence may be addressed. Email: l.enjuanes@cnb.csic.es.

Published October 22, 2021.

RNA replicons are promising platforms for vaccine generation (44). To amplify these replicons, it is necessary to provide the deleted gene(s) in *trans*. RNA replicons can be classified as replication defective or replication competent but propagation defective. Self-amplifying RNA replicons may achieve the same degree of protection as synthetic mRNA vaccines but use 64-fold lower doses of RNA (45). The most popular replicons are based on *Aplhaviruses* such as Semliki forest virus (46, 47), Sindbis virus (48), and Venezuelan equine encephalitis virus (49, 50). However, there are also replicons derived from viruses like West Nile virus (WNV) (51); Kunjin virus, a subtype of WNV (52, 53); measles virus (54–56); rabies virus (57, 58); vesicular stomatitis virus (59, 60); and bluetongue virus (61), among others (44).

In this manuscript, the development of CoV-based self-amplifying RNA replicons is described. These replicons have been generated by the deletion of the envelope (E) gene alone or together with up to four additional genes (3, 4a, 4b, 5). The *in vivo* evaluation of these RNA replicons demonstrated that they were safe and stable vaccine candidates that induced potent sterilizing immunity.

Materials and Methods

Ethics Statement. Animal experimental protocols were approved by the Environmental Council of Madrid (permit no. PROEX 112/14) and the Ethical Committee of Centro de Investigación en Sanidad Animal–Instituto Nacional de Investigación y Tecnología Agraria (CISA-INIA) (Madrid, Spain) (permit nos. CBS 2014/005 and CEEA 2014/004) in strict accordance with Spanish National Royal Decree (RD) 53/2013 and International European Union Guideline 2010/63/UE about the protection of animals used for experimentation and other scientific purposes and Spanish National Law 32/2007 about animal welfare. All work with infected animals was performed in a Biosafety Level 3+ laboratory of the CISA-INIA (Madrid, Spain). Infected mice were housed in a self-contained ventilated rack (Allentown, NJ).

Plasmids and Bacteria Strains. Bacterial artificial chromosome (BAC) pBeloBAC11 (62), provided by H. Shizuya, California Institute of Technology, Pasadena, CA, was used to assemble recombinant MERS-CoV and MERS-CoV mouse-adapted (MERS-MA30) infectious complementary DNA (cDNA) clones. This plasmid is a low–copy number plasmid (one, maximum two copies per cell) based on the *Escherichia coli* F factor (63) that allows the stable maintenance of large DNA fragments in bacteria. *E. coli* DH10B (Gibco/BRL) cells were transformed by electroporation using a MicroPulser unit (Bio-Rad) according to the manufacturer's instructions. BAC plasmid and recombinant BACs were isolated and purified using a large-construct kit (Qiagen), following the manufacturer's specifications.

Two plasmids were used for the expression of the MERS-CoV E protein: pcDNA3.1 for constitutive expression (Invitrogen; Thermo Fisher Scientific) (64) and TRE-Auto-rtTA-V10-2T for inducible expression provided by A. Das and B. Berkhout, Academisch Medisch Centrum Universiteit van Amsterdam, Amsterdam, The Netherlands (65).

Generation of Recombinant MERS-MA30 cDNA Clones. pBAC-MERS$_{FL}$-MA (66) was used as the basis for engineering the mutated recombinant MERS-MA30 used in this report: rMERS-MA30-ΔE (deletion of the gene E), rMERS-MA30-Δ[5,E] (deletion of the ORF5 and E genes), rMERS-MA30-Δ[3,4a,4b,5] (deletion of the ORF3, ORF4a, ORF4b, and ORF5 genes), and rMERS-MA30-Δ[3,4a,4b,5,E] (deletion of the ORF3, ORF4a, ORF4b, ORF5, and E genes). The pBAC-MERS$_{FL}$-MA-Δ5 has been described (66).

For the generation of the infectious cDNA of rMERS-MA30-ΔE and rMERS-MA30-Δ[5,E], a 502-bp fragment flanked by *Kfl*I and *Pfl*23II restriction sites was chemically synthetized (GeneArt; Thermo Fisher Scientific). This fragment included MERS-MA30 mutations (66, 67) between nucleotides 27535 and 28236 of the viral genome, the deletion of the core sequence of the transcription-regulating sequence (TRS) of gene E, and the deletion of the first 197 nucleotides of gene E. The last 52 nucleotides of gene E were maintained since these sequences include part of the M gene TRS. The synthetized fragment was cloned into the intermediate plasmid pBAC-SA-F6 (positions 25841 to 30162 of the viral genome) to generate pBAC-SA-F6-MA-ΔE and into pBAC-SA-F6-MA-Δ5 to generate pBAC-SA-F6-MA-Δ[5,E]. The *Pac*I-*Rsr*II fragments from pBAC-SA-F6-MA-ΔE and from pBAC-SA-F6-MA-Δ[5,E], which include the *Kfl*I-*Pfl*23II region, were cloned into pBAC-MERS$_{FL}$-MA to obtain pBAC-MERS$_{FL}$-MA-ΔE and pBAC-MERS$_{FL}$-MA-Δ[5,E], respectively.

For the construction of the infectious cDNA clone of rMERS-MA30-Δ[3,4a,4b,5,E] and rMERS-MA30-Δ[3,4a,4b,5], an intermediate plasmid, pUC57-F5-Δ3-MERS-MA, was previously generated from a pUC57-F5-Δ3-MERS (64). pUC57-F5-Δ3-MERS-MA includes mutations acquired by MERS-MA30 (66, 67) in the region of the viral genome between nucleotides 20902 and 25840, as well as the deletion of the ORF3 gene. This region, flanked by *Swa*I and *Pac*I restriction sites, was cloned into pBAC-MERS$_{FL}$-MA and pBAC-MERS$_{FL}$-MA-ΔE to obtain pBAC-MERS$_{FL}$-MA-Δ3 and pBAC-MERS$_{FL}$-MA-Δ[3,E]. These plasmids were digested with *Pac*I and *Kfl*I to delete the ORF4a, ORF4b, and ORF5 genes. The resultant fragments were separated by agarose gel electrophoresis and purified. Since the ends resulting from digestion were not cohesive with each other, blunt ends were generated with T4 phage DNA polymerase (New England Biolabs). For this, 300 ng of each digested and purified plasmid was incubated with 1 U of enzyme for each microgram of DNA for 30 min at 37 °C in the presence of an excess of deoxyribonucleotides triphosphate. The enzyme was then inactivated at 75 °C for 20 min, and phage T4 DNA ligase (Roche) was added to ligate the ends, generating pBAC-MERS$_{FL}$-MA-Δ[3,4a,4b,5] and pBAC-MERS$_{FL}$-MA-Δ[3,4a,4b,5,E] plasmids.

Cells. Human hepatocyte-derived carcinoma (Huh-7) and baby hamster kidney (BHK-21) cells were provided by R. Bartenschlager, University of Heidelberg, Heidelberg, Germany and H. Laude, Unité de Virologie et Immunologie Moléculaires, INRAE, Jouy-en-Josas, France, respectively. Cells were grown in Dulbecco's modified Eagle's medium (DMEM) with 25 mM 4-(2-hydroxyethyl)-1-piperazineethanesulfonic acid nd 4.5 g/L glucose (BioWhittaker; Lonza), supplemented with 4 mM glutamine, 1× nonessential amino acids (Sigma-Aldrich), and 10% vol/vol fetal bovine serum (FBS; HyClone; Thermo Scientific).

Viruses. Wild-type rMERS-CoV and rMERS-CoV-ΔE (EMC/2012 strain) (64) and parental virulent rMERS-MA30 (66) and rMERS-MA30–derived mutants were all rescued from infectious cDNA clones generated in a BAC. The viruses were then grown and titrated on Huh-7 cells using closed flasks or plates placed in sealed plastic bags, respectively. All the work was performed at Centro Nacional de Biotecnología - Consejo Superior de Investigaciones Científicas (CNB-CSIC, Madrid, Spain) biosafety level 3 facility (Madrid, Spain) following the security guidelines and standard procedures.

Recovery of Recombinant MERS-MA30 Mutants from the cDNA Clones. BHK-21 cells were grown to 95% confluence in 12.5-cm^2 flasks and transfected with 6 μg of each infectious cDNA clone and 18 μL of Lipofectamine 2000 (Invitrogen), according to the manufacturer's specifications. Three independent cDNA clones were recovered of each mutant. At 6 h posttransfection (hpt), cells were trypsinized, added to confluent Huh-7 cell monolayers grown in 12.5-cm^2 flasks, and incubated at 37 °C for 72 h (passage 0). Cell supernatants were harvested and passaged two times on fresh cells (passages 1 and 2). Viability, titer, and sequence of the mutants were analyzed to generate viral stocks for *in vitro* and *in vivo* evaluations.

To rescue viruses lacking the E gene, Huh-7 cells were transfected with pcDNA3.1-E-MERS-CoV or with TRE-Auto-rtTA-V10-2T-E-MERS-CoV, while BHK-21 cells were cotransfected with infectious cDNA and E protein expression plasmid. At 6 hpt, the medium containing the plasmid–Lipofectamine complexes was removed from the transfected Huh-7 cells and washed, and fresh medium was added. For cells transfected with the TRE-Auto-rtTA-V10-2T-E-MERS-CoV plasmid, the medium was supplemented with doxycycline at a concentration of 1 μg/mL. The transfected BHK-21 cells were trypsinized, detached from the flask, added to the Huh-7 cells transfected with the E protein expression plasmids, and incubated at 37 °C for 72 h. For successive virus amplification passages and virus stocks, Huh-7 cells were transfected with E protein expression plasmids in a DNA:Lipofectamine 2000 ratio of 1:3 (micrograms:microliters).

Transmission Electron Microscopy. Huh-7 cells were seeded in 24-well plates. After 24 h, cells were infected with MERS-CoV and rMERS-CoV-ΔE at different multiplicities of infection (MOIs; 1.0, 0.1, and 0.01). At 17 h postinfection (hpi), medium was removed, and cells were washed with phosphate-buffered saline (PBS) and fixed *in situ* for 2 h at room temperature (R/T) with a solution of 4% wt/vol paraformaldehyde and 2% wt/vol glutaraldehyde in Sörensen phosphate buffer 0.1 M at pH 7.4. Prefixed cells were stored at 4 °C for 24 h. Cells were processed directly in plates. For this, fixative was removed, and cells were embedded in TAAB 812 epoxy resin (TAAB Laboratories). Using the resin blocks, ultrathin (70- to 80-nm) sections were produced with an Ultracut E ultramicrotome (Leica). These cuts were treated with a solution of 2% uranyl acetate in water and Reynolds lead citrate. Sections were examined at 80 kV

in a transmission electron microscope JEM1010 (Jeol), and images were taken with a TemCam F416 complementary metal-oxide-semiconductor digital camera (Tietz Video and Image Processing Systems). The embedding, sectioning, placement in grids, and capture of images were carried out in the Electron Microscopy Service of Centro de Biología Molecular Severo Ochoa - Consejo Superior de Investigaciones Científicas–Universidad Autónoma de Madrid (CBMSO-CSIC-UAM) (Madrid, Spain).

Viral Titration by Focus-Forming Immunofluorescence Assay. In total, 5×10^4 Huh-7 cells were seeded per well in 96-well plates in 100 μL of media 1 d prior to the immunofluorescence assay. The next day, cells were infected with 20 μL of undiluted or serial 10-fold–diluted virus. At 16 hpi, cells were fixed with paraformaldehyde 4% wt/vol for 40 min, washed, and permeabilized with chilled methanol at R/T for 20 min. Nonspecific binding was blocked with FBS 10% in PBS for 1 h at R/T. Then, cells were incubated for 90 min at R/T with rabbit polyclonal antibody anti–*N*-MERS (Biogenes). Secondary monoclonal antibody goat anti-rabbit conjugated with Alexa 488 (Invitrogen) was incubated for 45 min to detect and count infectious foci of MERS-MA30 and rMERS-MA30 mutants. The titer was expressed as focus-forming units (FFUs) per milliliter.

Growth Kinetics. Subconfluent monolayers (90% confluence) of Huh-7 cells grown in 12.5-cm^2 flasks were infected at an MOI of 0.001 with the indicated viruses. Culture supernatants were collected at 0, 24, 48, and 72 hpi, and virus titers were determined as described above.

Mouse Strains, Virus Infection, and Growth *In Vivo*. MERS-CoV–susceptible transgenic B6;SJL-Tg(*K18-DPP4*) (K18-hDPP4) (68) and knock-in C57BL/6NTac-*Dpp4*$^{tm3600(DPP4)Arte}$ (hDPP4-KI) (67) mice were provided by Paul McCray, University of Iowa, Iowa City, IA. A colony of both strains was stablished in the CNB-CSIC animal care facility (Madrid, Spain); 16- to 24-wk-old female mice were anesthetized with isoflurane and intranasally inoculated with 50 μL of virus diluted in DMEM. Human MERS-CoV (EMC/2012 strain) and its derived mutants were evaluated in K18-hDPP4 mice using 5,000 FFU of the indicated virus per mouse to assess virulence and 50,000 FFU of virulent MERS-CoV virus in challenge experiments. Mouse-adapted MERS-CoV (MERS-MA30) and its derived mutants were evaluated in hDPP4-KI mice using 10,000 FFU of the indicated virus per mouse to examine attenuation and 100,000 FFU of virulent MERS-MA30 for challenge (66). Weight loss and mortality were evaluated daily. To determine viral titers, lungs were homogenized in 2 mL of PBS containing 100 IU/mL penicillin, 0.1 mg/mL streptomycin, 50 μg/mL gentamicin, and 0.5 μg/mL amphotericin B (Fungizone) using a gentleMACS dissociator (Miltenyi Biotec, Inc.). Virus titrations were performed in Huh-7 cells as described above. Viral titers were expressed as FFU counts per gram of tissue. All work with infected animals was performed in an Animal Biosafety Level 3+ laboratory (CISA-INIA, Madrid, Spain) wearing personal protection equipment (3M).

Extraction and Analysis of Viral RNA. RNA from infected cells or homogenized mouse lungs was collected and purified using an RNeasy kit (Qiagen). Total cDNA was synthesized using a High-Capacity cDNA Reverse Transcription Kit (ThermoFisher Scientific) with random hexamers and 150 ng of purified RNA in a final volume of 30 μL. cDNA products were subsequently subjected to PCR for sequencing using Vent polymerase (New England Biolabs). cDNA products from mouse lungs were analyzed by real-time quantitative PCR (qPCR) for viral RNA synthesis quantification. MERS-MA30 genomic RNA (forward primer 5'-GCACATCTGTGGTTCTCCTCTCT-3', reverse primer 5'-AAGCCCAGGCCCTACTATTAGC-3', and MGB probe 5'-TGCTCCAACAGTTACAC-3') and MERS-MA30 subgenomic messenger RNA (sgmRNA) N (forward primer 5'-CTTCCCCTCGTTCTCTTGCA-3', reverse primer 5'-TCATTGTTATCGGCAAAGGAAA-3', and MGB probe 5'-CTTTGATTTTAACGAATCTC-3') custom probes were designed for this analysis; forward and reverse primers were purchased from Sigma-Aldrich, and MGB probes were purchased from Eurofins Genomics. Data were acquired with a 7500 Real-Time PCR system (Applied Biosystems) and analyzed with ABI PRISM 7500 software, version 2.0.5. The relative quantifications were performed using the cycle threshold ($2^{-\Delta\Delta CT}$) method (69). To normalize differences in RNA sampling, the expression of mouse 18S ribosomal RNA was analyzed using a specific TaqMan Gene Expression Assay (Mm03928990_g1; ThermoFisher Scientific).

Histopathology. Mice were euthanized at the indicated day postinfection (dpi) or day postchallenge (dpc). The left lungs of infected mice were fixed in 10% zinc formalin for 24 h at 4 °C and paraffin embedded. Serial longitudinal 5-μm sections were stained with hematoxylin and eosin by the Histology Service at CNB-CSIC (Madrid, Spain) and subjected to histopathological examination with a ZEISS Axiophot fluorescence microscope. Samples were obtained using a systematic uniform random procedure, consisting of serial parallel slices made at a constant thickness interval of 50 μm. Histopathology analysis was conducted in a blind manner by acquiring images of 50 random microscopy fields from around 40 nonadjacent sections for each of the three independent mice analyzed per treatment group.

Stability of rMERS-MA30-Δ[3,4a,4b,5,E] Deletion Mutant. The stability of the rMERS-MA30-Δ[3,4a,4b,5,E] mutant was analyzed in Huh-7 cells in the absence or presence of E protein supplemented in trans with TRE-Auto-rtTA-V10-2T-E-MERS-CoV, as described above. Cells were seeded in 12.5-cm^2 flasks and infected with the mutant. Every 24 h, a third of the supernatant was used to infect a fresh lawn of cells. After each passage, the remaining supernatant was stored at −80 °C. Cells were lysed to extract RNA as described above. The 3' distal third of the rMERS-MA30-Δ[3,4a,4b,5,E] genome (spike, membrane, and nucleocapsid genes [S, M, and N]) was amplified by PCR, and the PCR product was purified by agarose electrophoresis and sequenced.

Virus Neutralization Assay. Blood samples were collected at 0 and 21 d after immunization from the submandibular vein. To facilitate the coagulation and the separation of the serum, blood samples were incubated at 37 °C for 1 h in a water bath and then placed overnight at 4 °C. The serum was clarified by centrifugation and stored frozen at −80 °C. One day before neutralization assay, 5×10^4 Huh-7 cells per well were seeded in 96-well plates. The next day, serum samples were thawed and incubated at 56 °C for 30 min to inactivate complement. Twofold dilutions of each serum were prepared in complete DMEM supplemented with 2% FBS in a final volume of 60 μL. Serum dilutions were incubated for 1 h at 37 °C with 100 tissue culture infectious dose 50% ($TCID_{50}$) of MERS-MA30 in a 1:1 proportion. Medium was removed from Huh-7 cells, and cells were incubated with 60 μL of serum:virus mixtures for 1 h at 37 °C. After incubation, the serum:virus mixture was replaced by fresh complete DMEM, and cells were incubated for 72 h at 37 °C. Finally, cells were fixed with formaldehyde 10% vol/vol and stained with crystal violet. Levels of neutralizing antibodies were determined in the serum of mice as the highest dilution showing complete neutralization of the cytopathic effect in 50% of the wells (TCID50).

Statistical Analysis. Two-tailed, unpaired Student's *t* tests were performed using GraphPad Prism version 6.00 for Mac (GraphPad Software; https://www.graphpad.com/) to analyze the differences in mean values between groups. All results were expressed as means ± SD, except weight losses, which were expressed as means ± SEM. P values < 0.05 were considered significant.

Results

Optimization of the Conditions for the Amplification of Recombinant Viruses Lacking the E Gene. Conditions for transient expression of E protein were optimized for the rescue and evaluation of RNA replicons derived from MERS-CoV mutants lacking the E gene. In order to select the appropriate rescue system, the expression levels of the E protein were compared in two different settings: constitutive expression using a pcDNA3.1-E-MERS-CoV plasmid (64) and an inducible expression system based on a plasmid containing a Tetracycline promoter (TRE-Auto-rtTA-V10-2T-E-MERS-CoV), which included a positive feedback loop (70). Huh-7 cells were transfected with similar amounts of each of the E protein expression plasmids. At 5 hpt, cells were infected at an MOI of 0.001 of MERS-CoV–wild type (WT) or the rMERS-CoV-ΔE replicon (EMC/2012 strain) (64). The expression of E protein was provided in cells transfected with the inducible plasmid TRE-Auto-rtTA-V10-2T-E-MERS-CoV by adding doxycycline at a concentration of 1 μg/mL. In the absence of E protein, the rMERS-CoV-ΔE replicon did not propagate (Fig. 1*A*). In cells expressing E protein, virus production at 24 hpi was similar in cells transfected with pcDNA3.1-E-MERS-CoV and those transfected with TRE-Auto-rtTA-V10-2T-E-MERS-CoV. At 72 hpi, MERS-CoV-ΔE titers increased 100-fold in cells transfected with pcDNA3.1-E-MERS-CoV compared with nontransfected cells. However, in cells transfected with TRE-Auto-rtTA-V10-2T-E-MERS-CoV, the titers of rMERS-CoV-ΔE increased more than 1,000-fold, reaching levels close to those of MERS-CoV-WT (Fig. 1*A*). Cells infected with MERS-CoV-WT and transfected with either

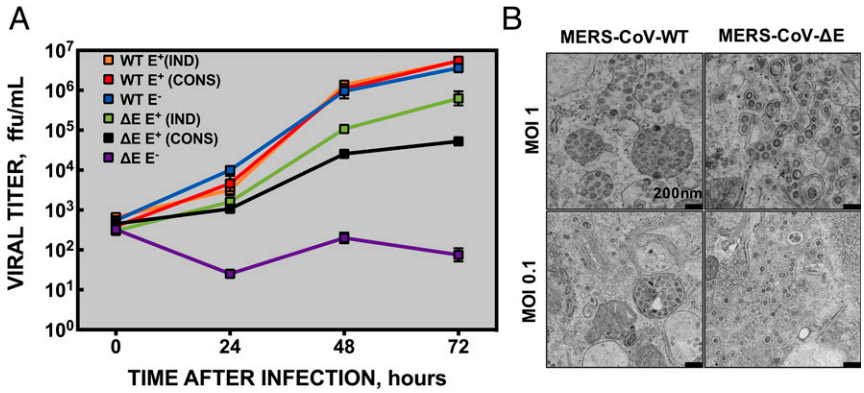

Fig. 1. Characterization of viral growth and morphogenesis of MERS-CoV lacking the E gene. (*A*) MERS-CoV-WT (WT) virus and rMERS-CoV-ΔE (ΔE) replicon growth were compared in Huh-7 cells transfected with plasmids constitutively (CONS; pcDNA-3.1-E-MERS-CoV) or inducibly (IND; TRE-Auto-rtTA-V10-2T-E-MERS) expressing E protein. Nontransfected cells (E^-) were used as the control for viral growth in the absence of E protein expression. Results are expressed as the mean ± SD. (*B*) For morphogenesis studies, Huh-7 cells without E protein complementation were infected at two MOIs, and samples were processed 17 h after infection. Large vesicles with a high concentration of spherical virions can be seen in MERS-CoV-WT–infected cells, with greater morphological alterations observed in cells infected at an MOI of one. MERS-CoV-ΔE–infected cells showed the vesicles with virions are in both conditions and lower cytopathic effect.

one of the two expression plasmids did not result in a significant increase of virus titers over nontransfected cells (Fig. 1*A*). These results showed that the TRE-Auto-rtTA-V10-2T-E-MERS-CoV plasmid facilitated optimal production of large amounts of MERS-CoV mutants lacking the E gene.

Virus-Like Particles Assembly by rMERS-CoV-ΔE Replicon in the Absence of the E Protein. The morphogenesis of MERS-CoV-WT virus and the rMERS-CoV-ΔE replicon was studied in the absence of E protein supplementation in Huh-7 cells infected at two different MOIs (Fig. 1*B*). At 17 hpi, cells were embedded in resin, and sections were taken for analysis by transmission electron microscopy (Fig. 1*B*). The rMERS-CoV-ΔE replicon led to the assembly of virions within the cell that resembled those of the MERS-CoV-WT virus. In cells infected at an MOI of one, MERS-CoV-WT virus showed greater morphological alterations, with vesicles full of virions with a spherical shape, while rMERS-CoV-ΔE replicon vesicles were less frequent, were elongated, and included a lower number of virus-like particles (VLPs). A similar observation was made in cells infected at an MOI of 0.1, although alterations of cell structures and organelles in MERS-CoV-WT infection were less obvious compared with the samples infected at an MOI of one. Given the similarity in size and shape of the viral structures formed by the rMERS-CoV-ΔE replicon compared with MERS-CoV-WT virus, immunization with the rMERS-CoV-ΔE replicon may trigger mechanisms and responses like those of natural infection, highlighting its immunogenic potential.

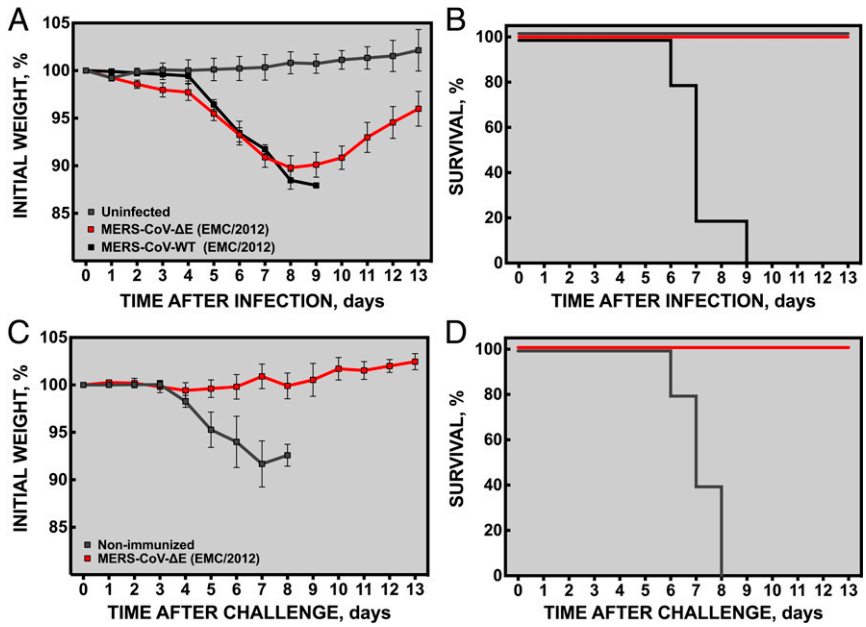

Fig. 2. In vivo evaluation of the EMC/2012 rMERS-CoV-ΔE replicon in a highly susceptible mouse model. K18-hDPP4 mice were infected with 5×10^3 FFU of MERS-CoV-WT virus or the rMERS-CoV-ΔE replicon and monitored for weight loss (*A*) and survival (*B*) for attenuation studies. After 21 dpim, nonimmunized and rMERS-CoV-ΔE–immunized mice were challenged with 5×10^4 FFU of MERS-CoV-WT per mouse, and (*C*) weight loss and (*D*) survival were monitored daily to evaluate the protection conferred by rMERS-CoV-ΔE against an MERS-CoV-WT lethal infection. Differences in weight loss are represented as mean ± SEM.

Evaluation of the rMERS-CoV-ΔE RNA Replicon (EMC/2012 Strain) *In Vivo*. The potential virulence of the rMERS-CoV-ΔE replicon *in vivo* was initially evaluated in K18-hDPP4 transgenic mice (68); 5×10^3 FFU in 50 μL of each virus were intranasally inoculated (Fig. 2 *A* and *B*). All mice infected with MERS-CoV-WT virus lost weight and died between 6 and 9 dpi. In contrast, mice intranasally inoculated with the rMERS-CoV-ΔE replicon survived, and the small weight that was initially lost was quickly regained, indicating that the rMERS-CoV-ΔE replicon was attenuated.

At 21 d postimmunization (dpim), mice inoculated with the rMERS-CoV-ΔE replicon were challenged with 5×10^4 FFU of rMERS-CoV-WT (Fig. 2 *C* and *D*). While all the unimmunized mice lost weight and died between 6 and 8 dpc, the mice immunized with rMERS-CoV-ΔE survived, and none of them suffered a significant weight loss. Together, these results demonstrated that a single immunization with 5×10^3 FFU of the rMERS-CoV-ΔE replicon was sufficient to protect against lethal infection with MERS-CoV-WT (EMC/2012) in highly susceptible K18-hDPP4 mice.

Construction and Viability of rMERS-MA30 Deletion Mutants Missing Several Nonessential Genes. Next, we introduced additional safety features into the replicon by preparing three replicons (lacking the E gene) and two recombinant viruses (maintaining the E gene) on a MERS-MA30 background. These constructs combined the deletion of accessory genes (ORF3, ORF4a, ORF4b, or ORF5) with the deletion of gene E: 1) rMERS-MA30-ΔE; 2) rMERS-MA30-Δ[5,E]; 3) rMERS-MA30-Δ[3,4a,4b,5,E]; 4) rMERS-MA30-Δ5; and 5) rMERS-MA30-Δ[3,4a,4b,5] (Fig. 3*A*). Recombinant mutants were engineered on a MERS-MA30 background because infection of hDPP4-KI mice with this mouse-adapted virus better reproduces the clinical signs of human MERS (67) compared with K18-hDPP4 mice infected with MERS-CoV EMC/2012, in which brain disease occurred (68). All mutants were rescued and viable. Replicons lacking the E gene were rescued in the presence of E protein provided in trans by Huh-7 cells transiently transfected with the inducible expression plasmid (TRE-Auto-rtTA-V10-2T-E-MERS-CoV).

Growth of the deletion mutants was evaluated in Huh-7 cells. In the absence of E protein, MERS-MA30 (WT) and rMERS-MA30-Δ5 viruses followed similar growth kinetics (Fig. 3*B*). A growth reduction was observed at 24 hpi after infection with rMERS-MA30-Δ[3,4a,4b,5] compared with MERS-MA30 and rMERS-MA30-Δ5 viruses (Fig. 3*B*), most likely due to the absence of accessory genes (71). rMERS-

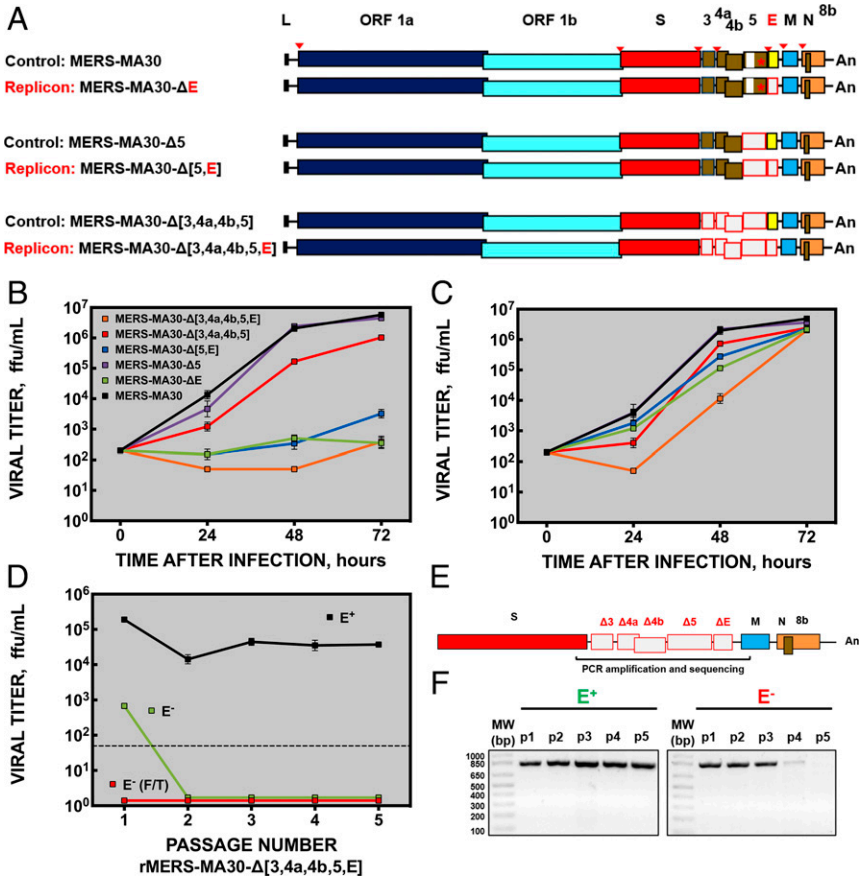

Fig. 3. Engineering and in vitro characterization of MERS-MA30 mutants lacking different sets of viral genes. (*A*) Scheme of deletion mutants engineered using the MERS-CoV mouse-adapted infectious cDNA clone (MERS-MA30). Virus genes are indicated at the top of the figure. White boxes indicate deleted genes. A deletion and a stop codon (red asterisks) in ORF5 were present in MERS-MA30 and the infectious cDNA clone developed from this virus (66). (*B* and *C*) Growth kinetics of viruses and replicons derived from MERS-MA30 in the absence (*B*) or in the presence (*C*) of the E protein provided in trans. Huh-7 cells were infected at an MOI of 0.001, and the infection was followed for 72 h. Results are expressed as mean ± SD. (*D*) Titration of the rMERS-MA30-Δ[3,4a,4b,5,E] replicon passed in Huh-7 cells in the presence or absence of E protein. Virus passages were performed in Huh-7 cells every 24 h. The presence of the replicon at passage 1 in E^- cells might be due to the initial inoculum. The detection limit was 50 FFU/mL (dashed black line). Results are expressed as mean ± SD. E^+, replicon supplemented with E protein of MERS-CoV-WT virus; E^-, replicon in the absence of E protein provided in trans; E^- (F/T), cells not supplemented with E protein were subjected to three freeze–thaw cycles to mechanically release the replicon. (*E*) Scheme of the MERS-MA30-Δ[3,4a,4b,5,E] replicon indicating the amplified region by PCR for sequencing and electrophoretic analyses. (*F*) Agarose gel electrophoresis showing the PCR products from passages 1 to 5 in Huh-7 cells in the presence or absence of E protein provided in trans. S: spike gene; M: membrane gene; N: nucleocapsid gene; An: polyadenylation tail; MW: molecular weight; bp: base pairs.

MA30-ΔE and rMERS-MA30-Δ[5,E] (Fig. 3*B*) replicons behaved similarly to the rMERS-CoV-ΔE replicon (EMC/2012 strain) (Fig. 1*A*). In contrast, replication was substantially diminished at 24 and 48 hpi in cells infected with the replicon in which all five genes were deleted (rMERS-MA30-Δ[3,4a,4b,5,E]) compared with rMERS-MA30-ΔE and rMERS-MA30-Δ[5,E] (Fig. 3*B*).

In the presence of the E protein provided in trans, MERS-MA30 (WT) and rMERS-MA30-Δ5 viruses grew similarly (Fig. 3*C*) to the same viruses grown in the absence of E protein (Fig. 3*B*). Likewise, titers of rMERS-MA30-Δ[3,4a,4b,5] mutant were just two to four times higher in the presence of E protein and remained below the titers of MERS-MA30 and rMERS-MA30-Δ5 viruses (Fig. 3*C*). However, titers of rMERS-MA30-ΔE and rMERS-MA30-Δ[5,E] replicons were significantly increased in the presence of E protein provided in trans, reaching levels similar to those of MERS-MA30 and rMERS-MA30-Δ5 viruses at 72 hpi. rMERS-MA30-Δ[3,4a,4b,5,E] showed a slower growth than rMERS-MA30-ΔE and rMERS-MA30-Δ[5,E], even in the presence of E protein provided in trans. However, at late times postinfection, rMERS-MA30-Δ[3,4a,4b,5,E] reached titers similar to those of MERS-MA30 and rMERS-MA30-Δ5 in the presence of the E protein (Fig. 3*C*), indicating that the absence of the accessory proteins delayed but did not prevent maximal replication.

MERS-MA30-Δ[3,4a,4b,5,E] Was Propagation Defective in the Absence of the E Protein Provided In Trans. To confirm that the rMERS-MA30-Δ[3,4a,4b,5,E] replicon was propagation deficient, we passed it serially five times in Huh-7 cells in the presence or absence of E protein. rMERS-MA30-Δ[3,4a,4b,5,E] replicon efficiently propagated during passage in the presence of E protein provided in trans. However, in its absence, the rMERS-MA30-Δ[3,4a,4b,5,E] replicon was undetectable in the supernatant by passage 2 (Fig. 3*D*). Additionally, we assessed for but could not find any intracellular rMERS-MA30-Δ[3,4a,4b,5,E] replicon, indicating that this RNA replicon requires E protein in trans to propagate and is not infectious when artificially released (Fig. 3*D*).

In order to examine the stability of the rMERS-MA30-Δ[3,4a,4b,5,E] replicon in cell culture and also assess whether it could recombine with the RNA encoding E protein transcribed from the expression plasmid, RNA from cell culture was extracted, and the region between the S and M genes within the rMERS-MA30-Δ[3,4a,4b,5,E] replicon was amplified by PCR and sequenced (Fig. 3*F*). After five passages in Huh-7, we found that it remained genetically stable with no evidence that rMERS-MA30-Δ[3,4a,4b,5,E] recombined with the RNA encoding the E protein. In the absence of E protein, the amount of rMERS-MA30-Δ[3,4a,4b,5,E] replicon RNA decreased during passage (Fig. 3*E*), in agreement with the titration results (Fig. 3*D*).

Evaluation of the Pathogenicity of MERS-MA30 Deletion Mutants in hDPP4-KI Mice. The pathogenicity of rMERS-MA30-Δ[3,4a,4b,5] virus and the rMERS-MA30-ΔE, rMERS-MA30-Δ[5,E], and rMERS-MA30-Δ[3,4a,4b,5,E] replicons was evaluated in hDPP4-KI mice (67). rMERS-MA30 was used as the reference virulent virus (WT); 1×10^4 FFU of each virus or RNA replicon were intranasally inoculated into mice, and weight loss and survival were monitored for 13 d (Fig. 4 *A* and *B*). All mice inoculated with rMERS-MA30 virus lost weight and died between 6 and 8 dpi. In contrast, none of the mice infected with rMERS-MA30-Δ[3,4a,4b,5] virus or with rMERS-MA30-ΔE, rMERS-MA30-Δ[5,E], or rMERS-MA30-Δ [3,4a,4b,5,E] replicons lost weight, and all of them survived, indicating that all the deletion mutants were attenuated.

To further characterize infected mice, virus titer, replication (genomic RNA), and transcription (N gene) levels were analyzed in lungs at 3 and 6 dpi. High virus titers were detected at 3 and 6 dpi in the lungs of mice infected with MERS-MA30 virus, but no virus growth was observed in the lungs of mice inoculated with the rMERS-MA30-Δ[3,4a,4b,5,E] replicon (Fig. 4*C*). This result was consistent with previous in vitro results showing that in the absence of the E gene, MERS-CoV did not spread from cell to cell. Levels of rMERS-MA30-Δ[3,4a,4b,5,E] RNA were significantly lower than those of rMERS-MA30 virus (Fig. 4 *D* and *E*). Overall, these data suggest that rMERS-MA30-Δ[3,4a,4b,5,E] replicated and transcribed sgmRNAs *in vivo* without spreading.

No significant pathological changes were observed in the lungs of mice infected with rMERS-MA30-Δ[3,4a,4b,5,E] at 3 dpi (Fig. 4*F*). In contrast, the lungs of mice infected with MERS-MA30 showed clear alveolar wall thickening and peribronchial cuffing. By 6 dpi, examination of lungs of rMERS-MA30–infected mice revealed generalized infiltration and parenchyma consolidation, as well as edema in the airspaces, whereas the lungs of mice infected with rMERS-MA30-Δ[3,4a,4b,5,E] replicon remained similar to those of uninfected mice.

Protection Elicited by MERS-MA30–Derived Deletion Mutants in hDPP4-KI Mice. To assess whether rMERS-MA30-Δ[3,4a,4b,5,E] would be a useful vaccine, hDPP4-KI mice were immunized with the different MERS-MA30 deletion mutants and challenged at 21 dpim with a lethal dose of MERS-MA30 (1×10^5 FFU per mouse) (Fig. 5 *A* and *B*). Nonimmunized mice lost weight and died between 6 and 7 dpc. However, all mice immunized with any of the deletion mutants survived the challenge, and none of them suffered significant weight loss.

Samples were obtained at 2, 4, and 6 dpc from the lungs of rMERS-MA30-Δ[3,4a,4b,5,E]–immunized, MERS-MA30–challenged mice to analyze viral titers, replication, and transcription. MERS-MA30 virus and genomic and subgenomic (N gene) RNA were detected in the lungs of the nonimmunized mice (Fig. 5 *C*–*E*). In contrast, levels of viral RNA in the lungs of mice immunized with rMERS-MA30-Δ[3,4a,4b,5,E] were significantly lower, and no infectious virus was detected at all times after challenge, indicating that rMERS-MA30-Δ[3,4a,4b,5,E] conferred sterilizing immunity (Fig. 5 *C*–*E*). In fact, while the lungs of nonimmunized mice showed cellular infiltrates and thickening of the interstitial membranes at 2 dpc, the appearance of edema at 4 dpc, and extensive cellular infiltration with edema and focal hemorrhages at 6 dpc, the lungs of immunized mice remained nearly normal in appearance (Fig. 5*F*).

Levels of neutralizing antibodies were determined in the serum of immunized mice at 0 and 21 dpim by neutralization assay. Titers were expressed as the highest dilution showing complete neutralization of the cytopathic effect in 50% of the wells ($TCID_{50}$) (Fig. 5*G*). As expected, no neutralizing antibodies were detected in the serum of nonimmunized and rMERS-MA30-Δ[3,4a,4b,5,E]–immunized mice at 0 dpim. However, at 21 dpim, mice immunized with the rMERS-MA30-Δ[3,4a,4b,5,E] replicon showed significative levels of neutralizing antibodies compared with nonimmunized mice after one single immunization.

Together, these results demonstrated that rMERS-MA30-Δ[3,4a,4b,5] virus and rMERS-MA30-ΔE, rMERS-MA30-Δ[5,E], and rMERS-MA30-Δ[3,4a,4b,5,E] replicons induced protection in hDPP4-KI mice against a lethal dose of MERS-MA30 virus and that the rMERS-MA30-Δ[3,4a,4b,5,E] replicon promoted sterilizing immunity with significant levels of neutralizing antibodies.

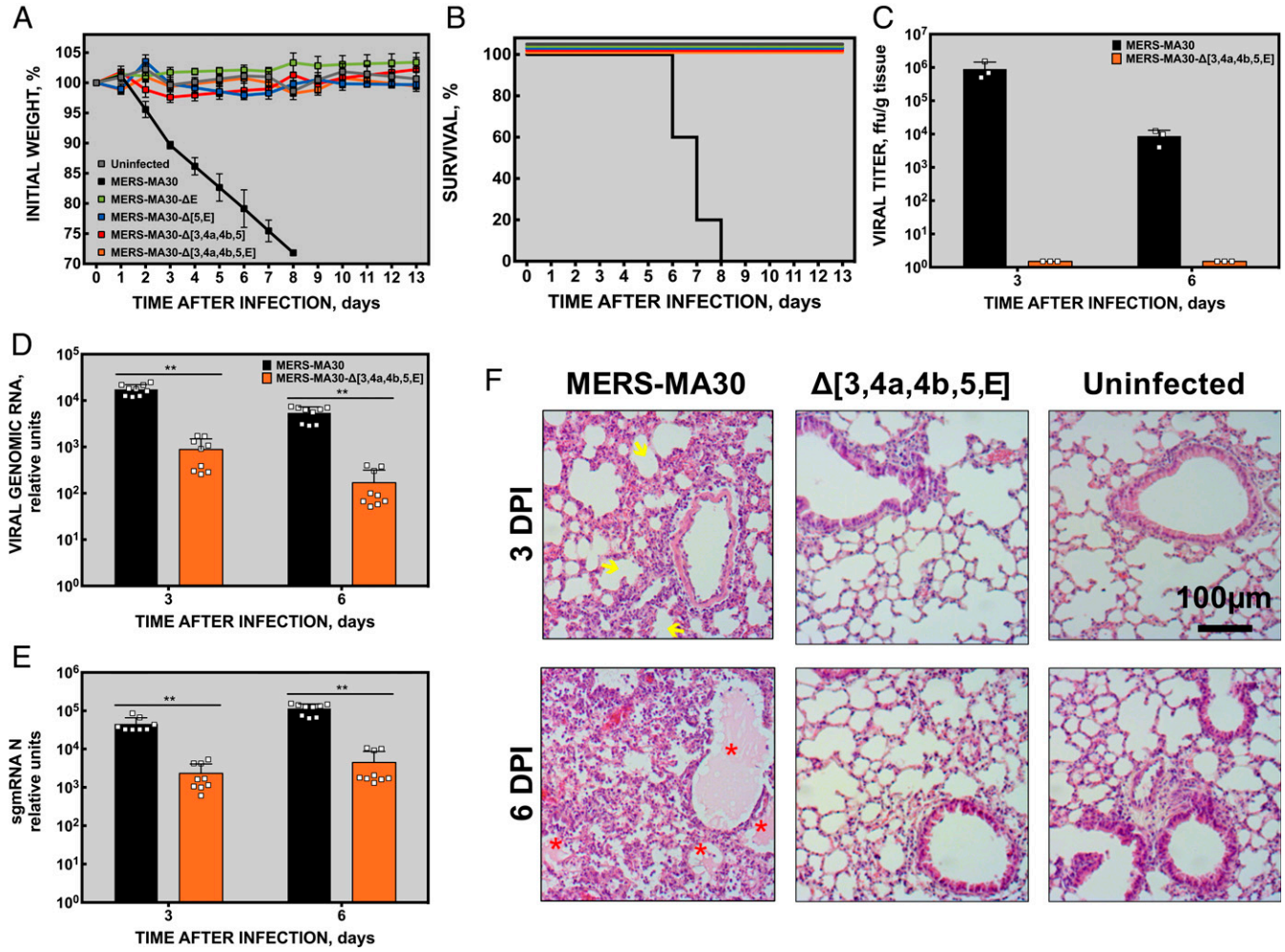

Fig. 4. Evaluation of rMERS-MA30–derived mutants and replicons attenuation in hDDP4-KI mice. Mice were infected with 1×10^4 FFU of each virus or replicon, and (*A*) weight loss and (*B*) survival were monitored. Differences in weight loss are represented as mean ± SEM. (*C*) Titers of MERS-MA30 virus or the rMERS-MA30-Δ[3,4a,4b,5,E] replicon in the lungs of infected mice. (*D*) Viral genomic RNA and (*E*) subgenomic RNA N in the lungs of infected mice. The results are expressed as mean ± SD. **Student's *t* test: significance level is lower than 0.01. (*F*) Histopathology induced by MERA-MA30 or the rMERS-MA30-Δ[3,4a,4b,5,E] replicon in the lungs of infected mice. In the lungs of the mice infected with rMERS-MA30, cell infiltrates and thickening of the alveoli walls (yellow arrows) were observed at 3 dpi, with the appearance of edema (red asterisks) and general lung infiltration at 6 dpi. The lungs of mice infected with the rMERS-MA30-Δ[3,4a,4b,5,E] replicon remained healthy and looked similar to the lungs of the uninfected mice.

Discussion

In this manuscript, we generated a series of MERS-CoV deletion mutants, many of which could not be propagated and showed that they were attenuated *in vivo*. The deletion of the E gene by itself resulted in a defect in propagation but not replication. Deletion of one or more accessory proteins should provide additional biosafety, as deletion of E or accessory ORFs (3, 4a, 4b, 5) attenuated the virus, increasing the safety profile of the designed vaccine candidate. Immunization with the nonpropagating constructs conferred full protection against a lethal dose of virulent MERS-MA30. We also showed that immunization with rMERS-MA30-Δ[3,4a,4b,5,E] elicited sterilizing immunity after a single vaccination dose, highlighting MERS-CoV–based RNA replicons as promising vaccine candidates.

RNA replicons combine the advantages of two classic vaccine types. They are almost as safe as inactivated vaccines since they cannot propagate, and their ability to amplify their genomes generated a protective response as high as the ones elicited by live attenuated vaccines as shown in this manuscript. The attenuation and safety of the rMERS-MA30-Δ[3,4a,4b,5,E] replicon can be improved by the introduction of partial deletions within the nsp1 nonstructural protein, as we have shown for SARS-CoV in which these deletions further attenuated the virus (72). Similarly, additional attenuation of the virus could be increased by mutations in the viral nsp16 protein, the 2-*O*' methyl transferase, which is important for immune evasion (73).

The deletion of nonessential genes (3, 4a, 4b, 5) showed a reduction in viral replication in both the rMERS-CoV-Δ[3,4a,4b,5,E] replicon complemented with E protein in trans and rMERS-CoV-Δ[3,4a,4b,5] virus. This reduction could be mainly due to ORF4ab deletion rather than ORF3 or ORF5 deletion, as previously reported (64, 74). Deletion of ORF3 and ORF5, along with ORF4ab and E gene, may reduce the possibility of recombination with other circulating MERS-like CoVs or human CoVs (75–81) or most importantly, with the E gene present in packaging cell lines since in the absence of homologous flanking sequences within the rMERS-MA30-Δ[3,4a,4b,5,E] replicon genome, it would be very unlikely to restore the E gene. Furthermore, the accessory genes are implicated in virulence (74, 82–87), and their deletion resulted in increased attenuation by a loss of function as demonstrated in in vivo experiments.

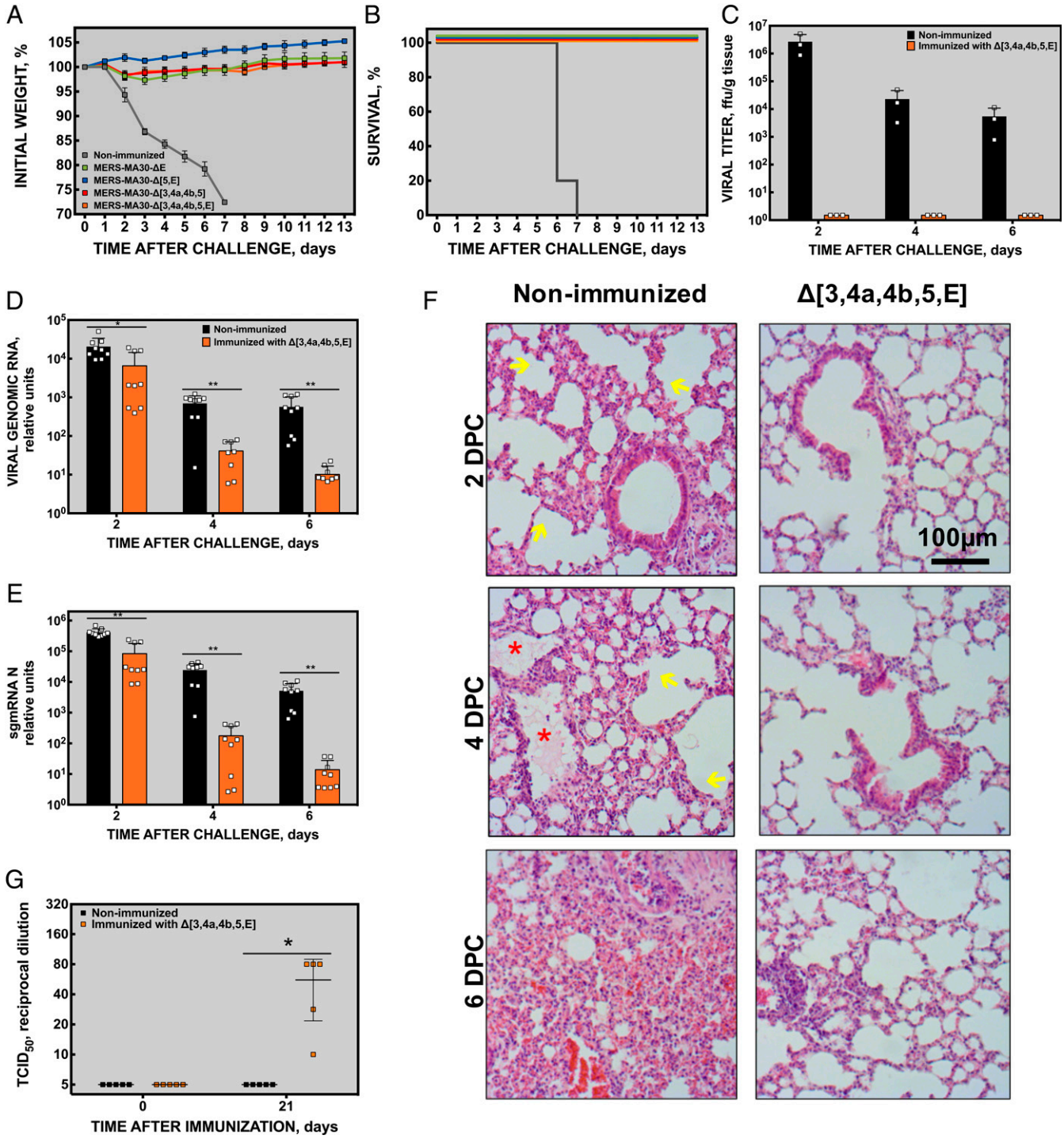

Fig. 5. Protection conferred by rMERS-MA30–derived mutants and replicons in hDPP4-KI mice. Mice were infected with the indicated viruses or replicons and challenged 21 d later with 10^5 FFU of MERS-MA30 per mouse. (*A*) Weight loss and (*B*) survival were monitored. Differences in weight loss are represented as mean ± SEM. (*C*) Titers of MERS-MA30 challenge virus in the lungs of nonimmunized mice and mice immunized with the rMERS-MA30-Δ[3,4a,4b,5,E] replicon. (*D*) Viral replication and (*E*) transcription in challenged mice. The results are expressed as mean ± SD. *Student's *t* test: significance level lower than 0.05; **Student's *t* test: significance level lower than 0.01. (*F*) Histopathology of immunized and nonimmunized mice challenged with MERS-MA30 virus. The lungs of the mice immunized with the rMERS-MA30-Δ[3,4a,4b,5,E] replicon looked healthy throughout the experiment. In the lungs of nonimmunized mice, peribronchial cuffing and alveolar thickening (yellow arrows) could be seen at 2 dpc. At 4 dpc, edema (red asterisks) could be observed in some air spaces, while at 6 dpc, highly evident edema, general cell infiltration, and focal hemorrhage could be observed. (*G*) Levels of neutralizing antibodies in the serum of immunized mice. Blood samples were taken from nonimmunized and rMERS-MA30-Δ[3,4a,4b,5,E]–immunized mice at 0 and 21 dpim to quantify neutralizing antibodies. Titers were expressed as the highest serum dilution showing complete neutralization of the cytopathic effect in 50% of the wells (TCID50). *Student's *t* test: *P* value = 0.0102919.

The deletion of additional nonessential genes, such as 3 and 5, in the RNA replicon did not affect replicon titers but reduced the possibility of recombination with other human CoVs, such as 229-E, OC43, NL-63, HKU-5, or SARS-CoV-2, and MERS-like CoVs circulating in the field (75–81). In addition, the accessory genes are implicated in virulence (74, 82–87), and their deletion resulted in increased attenuation by a loss of function.

The deletion of the E protein is key for virus attenuation since rMERS-CoV-ΔE is propagation deficient (64, 88). This characteristic of E^- replicons is a consequence of the role of this protein in intracellular transport, virus morphogenesis, and virion release from the cell (89–92). Another contribution of the deletion of E gene to biosafety is the elimination of several virulence motifs. One is related to the ability of E protein to form pentamers with ion channel activity (93). We have previously shown that the introduction of point mutations in the transmembrane domain of SARS-CoV E protein disrupts this activity (94). A second virulence factor present in E protein is the PDZ-binding motif (PBM), which maps at the end of the carboxy-terminus domain of E protein (72, 95). The PBM has a core sequence of four amino acids that can potentially bind to more than 400 cellular proteins, including syntenin (95, 96). Binding of SARS-CoV E protein to syntenin leads to the activation of p38MAPK by phosphorylation, activating the expression of several cytokines and exacerbating proinflammatory responses (95). The replacement of these four amino acids by glycine, or its deletion, leads to an attenuated virus (72, 95). Recently, we described that a forkhead-associated binding motif, present in the carboxy-terminus domain of MERS-CoV E protein, is likely implicated in virulence (90).

A total of 10^4 FFU per mouse were intranasally inoculated in a final volume of 50 μL. This volume can easily reach lung lobes, where genomic and subgenomic RNAs of MERS-MA30-WT virus and the rMERS-CoV-Δ[3,4a,4b,5,E] replicon were detected as shown in the manuscript (Fig. 4 *D* and *E*). Replication and transcription of MERS-MA30 propagation-defective replicons occurred in the lower respiratory tract. Initially, only cells infected with rMERS-CoV-Δ[3,4a,4b,5,E] replicon would replicate and transcribe its genome and sgmRNAs, as no infectious virus can be released from these cells. Nevertheless, cells neighboring replicon-infected cells might form syncytia, as expression of the S gene by itself induced its formation as previously shown in cell culture (97), slightly enhancing the synthesis replicon's RNA and sgmRNAs.

The safety of MERS-CoV–based RNA replicons was reinforced by the observation that VLPs (Fig. 1*B*) harboring RNA replicons in the absence of E protein complementation were noninfectious, even when these VLPs were artificially released from infected cells by freeze–thawing. However, they can induce syncytia formation in Huh-7 cells (90). This observation was expected, as it has been described that overexpression of MERS-CoV protein S induces syncytia formation in cell cultures (98). In addition, it has been shown that the membrane fusion peptide domain of the S2 subunit of the S protein is involved in the induction of syncytia formation (97). A tentative possibility to increase the safety of the rMERS-CoV-Δ[3,4a,4b,5,E] replicon would be mutation of this site responsible for syncytia formation, in order to inhibit replicon spread to the neighbor cells. Nevertheless, this potential modification of the replicon should take into consideration the deleterious effect on replicon infectivity, as prefusion conformation of S protein would not allow replicon infection, replication, and transcription, rendering a limited immunogen.

The insertion of transgenes or micro-RNAs may modulate or enhance the immune response elicited by the replicon (99), opening several possibilities for the design of advanced vaccines that may improve the immune response in those individuals with a weakened immune system, such as the elderly (99). We showed that certain miRNAs can modulate the growth of the virus and attenuate its pathogenicity in the context of SARS-CoV infection (100).

Viruses are the major generators of genetic variability in different species, including humans, by interchanging sequences (101, 102). CoVs, with the largest genome known among RNA viruses, have incorporated a proofreading system within their replication–transcription machinery (103) but still generate a high variability probably favored by the discontinuous RNA synthesis during the production of subgenomic RNAs, a process mediated by a high-frequency recombination event (104). This mechanism may facilitate the evolution of CoVs, generating a variety of novel animal and human pathogens. In fact, the emergence of novel animal and human highly pathogenic CoVs has been widely documented. Since different species of bats that fly across all continents act as a natural reservoir for these CoVs, the emergence or reemergence of deadly CoVs is a likely event for which we should be prepared by, among other things, the development of efficient vaccines. In this manuscript, it has been shown how through the application of reverse genetics procedures, the engineering of highly safe CoV-derived RNA replicons resulted in vaccine candidates inducing sterilizing immunity by a single intranasal dose administration. A similar strategy could be applied, in principle, to the development of vaccines against other highly pathogenic CoVs.

Data Availability. All study data are included in the main text.

ACKNOWLEDGMENTS. We thank Stanley Perlman for critical review of the manuscript and Marga Gonzalez from CNB-CSIC (Madrid, Spain) for her technical assistance. In vivo experiments were performed at CISA-INIA (Madrid, Spain). This work was supported by Government of Spain and European Union co-financed grant BIO2016-75549-R; by Government of Spain grants PID2019-107001RB-I00, Proyecto Intramural Especial (PIE) 202020E079, and PIE–Consejo Superior de Investigaciones Científicas (CSIC) 202020E043; by European Commission grants ZAPI_IMI_JU_115760, ISOLDA_848166, and MANCO_101003651; and by IH grant 2P01AI060699. The funders had no role in study design, data collection and analysis, decision to publish, or preparation of the manuscript.

1. A. E. Gorbalenya *et al.*, Coronaviridae Study Group of the International Committee on Taxonomy of Viruses, The species Severe acute respiratory syndrome-related coronavirus: Classifying 2019-nCoV and naming it SARS-CoV-2. *Nat. Microbiol.* **5**, 536–544 (2020).
2. R. J. de Groot *et al.*, Middle East respiratory syndrome coronavirus (MERS-CoV): Announcement of the Coronavirus Study Group. *J. Virol.* **87**, 7790–7792 (2013).
3. International Committee on Taxonomy of Viruses, ICTV Master Species List 2019.v1 (2019). https://talk.ictvonline.org/files/master-species-lists/m/msl/9601. Accessed 9 June 2021.
4. S. E. Colina, M. S. Serena, M. G. Echeverría, G. E. Metz, Clinical and molecular aspects of veterinary coronaviruses. *Virus Res.* **297**, 198382 (2021).
5. V. M. Corman, D. Muth, D. Niemeyer, C. Drosten, Hosts and sources of endemic human coronaviruses. *Adv. Virus Res.* **100**, 163–188 (2018).
6. A. Banerjee, K. Kulcsar, V. Misra, M. Frieman, K. Mossman, Bats and coronaviruses. *Viruses* **11**, 41 (2019).
7. J. Cui, F. Li, Z. L. Shi, Origin and evolution of pathogenic coronaviruses. *Nat. Rev. Microbiol.* **17**, 181–192 (2019).
8. V. Zappulli *et al.*, Pathology of coronavirus infections: A review of lesions in animals in the one-health perspective. *Animals (Basel)* **10**, 2377 (2020).
9. S. B. Polak, I. C. Van Gool, D. Cohen, J. H. von der Thüsen, J. van Paassen, A systematic review of pathological findings in COVID-19: A pathophysiological timeline and possible mechanisms of disease progression. *Mod. Pathol.* **33**, 2128–2138 (2020).
10. J. M. van den Brand, S. L. Smits, B. L. Haagmans, Pathogenesis of Middle East respiratory syndrome coronavirus. *J. Pathol.* **235**, 175–184 (2015).
11. S. Perlman, J. Netland, Coronaviruses post-SARS: Update on replication and pathogenesis. *Nat. Rev. Microbiol.* **7**, 439–450 (2009).
12. P. A. Rota *et al.*, Characterization of a novel coronavirus associated with severe acute respiratory syndrome. *Science* **300**, 1394–1399 (2003).
13. C. Drosten *et al.*, Identification of a novel coronavirus in patients with severe acute respiratory syndrome. *N. Engl. J. Med.* **348**, 1967–1976 (2003).

14. A. M. Zaki, S. van Boheemen, T. M. Bestebroer, A. D. Osterhaus, R. A. Fouchier, Isolation of a novel coronavirus from a man with pneumonia in Saudi Arabia. *N. Engl. J. Med.* **367**, 1814–1820 (2012).
15. N. Zhu *et al.*; China Novel Coronavirus Investigating and Research Team, A novel coronavirus from patients with pneumonia in China, 2019. *N. Engl. J. Med.* **382**, 727–733 (2020).
16. B. Hu, H. Guo, P. Zhou, Z. L. Shi, Characteristics of SARS-CoV-2 and COVID-19. *Nat. Rev. Microbiol.* **19**, 141–154 (2021).
17. World Health Organization, Summary of probable SARS cases with onset of illness from 1 November 2002 to 31 July 2003. https://www.who.int/publications/m/item/summary-of-probable-sars-cases-with-onset-of-illness-from-1-november-2002-to-31-july-2003. Accessed 26 April 2021.
18. European Centre for Disease Prevention and Control, MERS-CoV worldwide overview. https://www.ecdc.europa.eu/en/middle-east-respiratory-syndrome-coronavirus-mers-cov-situation-update. Accessed 26 April 2021.
19. Worldometer, COVID-19 coronavirus pandemic. https://www.worldometers.info/coronavirus/. Accessed 26 April 2021.
20. L. Du, W. Tai, Y. Zhou, S. Jiang, Vaccines for the prevention against the threat of MERS-CoV. *Expert Rev. Vaccines* **15**, 1123–1134 (2016).
21. C. Y. Yong, H. K. Ong, S. K. Yeap, K. L. Ho, W. S. Tan, Recent advances in the vaccine development against Middle East respiratory syndrome-coronavirus. *Front. Microbiol.* **10**, 1781 (2019).
22. P. M. Folegatti *et al.*, Safety and immunogenicity of a candidate Middle East respiratory syndrome coronavirus viral-vectored vaccine: A dose-escalation, open-label, non-randomised, uncontrolled, phase 1 trial. *Lancet Infect. Dis.* **20**, 816–826 (2020).
23. T. Koch *et al.*, Safety and immunogenicity of a modified vaccinia virus Ankara vector vaccine candidate for Middle East respiratory syndrome: An open-label, phase 1 trial. *Lancet Infect. Dis.* **20**, 827–838 (2020).
24. K. Modjarrad *et al.*, Safety and immunogenicity of an anti-Middle East respiratory syndrome coronavirus DNA vaccine: A phase 1, open-label, single-arm, dose-escalation trial. *Lancet Infect. Dis.* **19**, 1013–1022 (2019).
25. ClinicalTrials.gov, NCT04130594: Study of safety and immunogenicity of BVRS-GamVac. https://clinicaltrials.gov/ct2/show/NCT04130594?term=vaccine&recrs=abe&cond= MERS+%28Middle+East+Respiratory+Syndrome%29&draw=2&rank=5. Accessed 23 May 2021.
26. ClinicalTrials.gov, NCT04128059: Study of safety and immunogenicity of BVRS-GamVac-Combi. https://clinicaltrials.gov/ct2/show/NCT04128059?term=vaccine&recrs=abe&cond=MERS+% 28Middle+East+Respiratory+Syndrome%29&draw=2&rank=6. Accessed 23 May 2021.
27. ClinicalTrials.gov, NCT04119440: Safety and immunogenicity of the candidate vaccine MVA-MERS-S_DF-1 against MERS (MVA-MERS-S). https://clinicaltrials.gov/ct2/show/NCT04119440?term= vaccine&recrs=abe&cond=MERS+%28Middle+East+Respiratory+Syndrome%29& draw=2. Accessed 23 May 2021.
28. J. H. Beigel *et al.*, Safety and tolerability of a novel, polyclonal human anti-MERS coronavirus antibody produced from transchromosomic cattle: A phase 1 randomised, double-blind, single-dose-escalation study. *Lancet Infect. Dis.* **18**, 410–418 (2018).
29. H. Mou *et al.*, The receptor binding domain of the new MERS coronavirus maps to a 231-residue region in the spike protein that efficiently elicits neutralizing antibodies. *J. Virol.* **87**, 9379–9383 (2013).
30. V. S. Raj *et al.*, Dipeptidyl peptidase 4 is a functional receptor for the emerging human coronavirus-EMC. *Nature* **495**, 251–254 (2013).
31. C. Ma *et al.*, Intranasal vaccination with recombinant receptor-binding domain of MERS-CoV spike protein induces much stronger local mucosal immune responses than subcutaneous immunization: Implication for designing novel mucosal MERS vaccines. *Vaccine* **32**, 2100–2108 (2014).
32. N. Zhang *et al.*, Identification of an ideal adjuvant for receptor-binding domain-based subunit vaccines against Middle East respiratory syndrome coronavirus. *Cell. Mol. Immunol.* **13**, 180–190 (2016).
33. S. Pierini *et al.*, Trial watch: DNA-based vaccines for oncological indications. *OncoImmunology* **6**, e1398878 (2017).
34. J. J. Suschak, J. A. Williams, C. S. Schmaljohn, Advancements in DNA vaccine vectors, non-mechanical delivery methods, and molecular adjuvants to increase immunogenicity. *Hum. Vaccin. Immunother.* **13**, 2837–2848 (2017).
35. D. Hobernik, M. Bros, DNA vaccines-How far from clinical use? *Int. J. Mol. Sci.* **19**, 3605 (2018).
36. U. Sahin, K. Karikó, Ö. Türeci, mRNA-based therapeutics—developing a new class of drugs. *Nat. Rev. Drug Discov.* **13**, 759–780 (2014).
37. F. P. Polack *et al.*, C4591001 Clinical Trial Group, Safety and efficacy of the BNT162b2 mRNA Covid-19 vaccine. *N. Engl. J. Med.* **383**, 2603–2615 (2020).
38. L. R. Baden *et al.*, COVE Study Group, Efficacy and safety of the mRNA-1273 SARS-CoV-2 vaccine. *N. Engl. J. Med.* **384**, 403–416 (2021).
39. Pfizer, Pfizer-Biotech COVID-19 vaccine (also known as BNT162B2). https://www.pfizer.com/products/product-detail/pfizer-biontech-covid-19-vaccine. Accessed 23 May 2021.
40. Moderna, Moderna COVID-19 vaccine. https://www.modernatx.com/covid19vaccine-eua/. Accessed 23 May 2021.
41. A. Pandey *et al.*, Impact of preexisting adenovirus vector immunity on immunogenicity and protection conferred with an adenovirus-based H5N1 influenza vaccine. *PLoS One* **7**, e33428 (2012).
42. K. McCoy *et al.*, Effect of preexisting immunity to adenovirus human serotype 5 antigens on the immune responses of nonhuman primates to vaccine regimens based on human- or chimpanzee-derived adenovirus vectors. *J. Virol.* **81**, 6594–6604 (2007).
43. L. H. Haut, S. Ratcliffe, A. R. Pinto, H. Ertl, Effect of preexisting immunity to adenovirus on transgene product-specific genital T cell responses on vaccination of mice with a homologous vector. *J. Infect. Dis.* **203**, 1073–1081 (2011).
44. K. Lundstrom, Self-amplifying RNA viruses as RNA vaccines. *Int. J. Mol. Sci.* **21**, 5130 (2020).
45. A. B. Vogel *et al.*, Self-amplifying RNA vaccines give equivalent protection against influenza to mRNA vaccines but at much lower doses. *Mol. Ther.* **26**, 446–455 (2018).
46. P. Liljeström, H. Garoff, A new generation of animal cell expression vectors based on the Semliki Forest virus replicon. *Biotechnology (N. Y.)* **9**, 1356–1361 (1991).
47. A. R. Sánchez-Paulete *et al.*, Intratumoral immunotherapy with XCL1 and sFlt3L encoded in recombinant Semliki Forest virus-derived vectors fosters dendritic cell-mediated T-cell cross-priming. *Cancer Res.* **78**, 6643–6654 (2018).
48. K. Lundstrom, Alphavirus-based vaccines. *Methods Mol. Biol.* **1404**, 313–328 (2016).
49. C. K. Jurgens, K. R. Young, V. J. Madden, P. R. Johnson, R. E. Johnston, A novel self-replicating chimeric lentivirus-like particle. *J. Virol.* **86**, 246–261 (2012).
50. S. Agnihothram *et al.*, Development of a broadly accessible Venezuelan equine encephalitis virus replicon particle vaccine platform. *J. Virol.* **92**, e00027-18 (2018).
51. D. G. Widman, I. Frolov, P. W. Mason, Third-generation flavivirus vaccines based on single-cycle, encapsidation-defective viruses. *Adv. Virus Res.* **72**, 77–126 (2008).
52. O. Reynard *et al.*, Kunjin virus replicon-based vaccines expressing Ebola virus glycoprotein GP protect the guinea pig against lethal Ebola virus infection. *J. Infect. Dis.* **204** (suppl. 3), S1060–S1065 (2011).
53. T. J. Harvey *et al.*, Kunjin virus replicon vectors for human immunodeficiency virus vaccine development. *J. Virol.* **77**, 7796–7803 (2003).
54. W. W. Leitner *et al.*, Alphavirus-based DNA vaccine breaks immunological tolerance by activating innate antiviral pathways. *Nat. Med.* **9**, 33–39 (2003).
55. M. D. Mühlebach, Vaccine platform recombinant measles virus. *Virus Genes* **53**, 733–740 (2017).
56. Q. Wang, A. Vossen, Y. Ikeda, P. Devaux, Measles vector as a multigene delivery platform facilitating iPSC reprogramming. *Gene Ther.* **26**, 151–164 (2019).
57. M. C. Leslie *et al.*, Immunization against MUC18/MCAM, a novel antigen that drives melanoma invasion and metastasis. *Gene Ther.* **14**, 316–323 (2007).
58. K. Lundstrom, Self-replicating RNA viruses for RNA therapeutics. *Molecules* **23**, 3310 (2018).
59. X. Yin *et al.*, Synergistic antitumor efficacy of combined DNA vaccines targeting tumor cells and angiogenesis. *Biochem. Biophys. Res. Commun.* **465**, 239–244 (2015).
60. R. Yamanaka, K. G. Xanthopoulos, Induction of antigen-specific immune responses against malignant brain tumors by intramuscular injection of sindbis DNA encoding gp100 and IL-18. *DNA Cell Biol.* **24**, 317–324 (2005).
61. E. Matsuo *et al.*, Generation of replication-defective virus-based vaccines that confer full protection in sheep against virulent bluetongue virus challenge. *J. Virol.* **85**, 10213–10221 (2011).
62. K. Wang, C. Boysen, H. Shizuya, M. I. Simon, L. Hood, Complete nucleotide sequence of two generations of a bacterial artificial chromosome cloning vector. *Biotechniques* **23**, 992–994 (1997).
63. H. Shizuya *et al.*, Cloning and stable maintenance of 300-kilobase-pair fragments of human DNA in *Escherichia coli* using an F-factor-based vector. *Proc. Natl. Acad. Sci. U.S.A.* **89**, 8794–8797 (1992).
64. F. Almazán *et al.*, Engineering a replication-competent, propagation-defective Middle East respiratory syndrome coronavirus as a vaccine candidate. *MBio* **4**, e00650–e13 (2013).
65. A. T. Das, X. Zhou, S. W. Metz, M. A. Vink, B. Berkhout, Selecting the optimal Tet-On system for doxycycline-inducible gene expression in transiently transfected and stably transduced mammalian cells. *Biotechnol. J.* **11**, 71–79 (2016).
66. J. Gutierrez-Alvarez *et al.*, Middle East respiratory syndrome coronavirus gene 5 modulates pathogenesis in mice. *J. Virol.* **95**, e01172–e01120 (2021).
67. K. Li *et al.*, Mouse-adapted MERS coronavirus causes lethal lung disease in human DPP4 knockin mice. *Proc. Natl. Acad. Sci. U.S.A.* **114**, E3119–E3128 (2017).
68. K. Li *et al.*, Middle East respiratory syndrome coronavirus causes multiple organ damage and lethal disease in mice transgenic for human dipeptidyl peptidase 4. *J. Infect. Dis.* **213**, 712–722 (2016).
69. K. J. Livak, T. D. Schmittgen, Analysis of relative gene expression data using real-time quantitative PCR and the 2(-Delta C(T)) method. *Methods* **25**, 402–408 (2001).
70. A. T. Das, L. Tenenbaum, B. Berkhout, Tet-On systems for doxycycline-inducible gene expression. *Curr. Gene Ther.* **16**, 156–167 (2016).
71. V. D. Menachery *et al.*, MERS-CoV accessory ORFs play key role for infection and pathogenesis. *MBio* **8**, e00665–e00617 (2017).
72. J. A. Regla-Nava *et al.*, Severe acute respiratory syndrome coronaviruses with mutations in the E protein are attenuated and promising vaccine candidates. *J. Virol.* **89**, 3870–3887 (2015).
73. V. D. Menachery *et al.*, Middle East respiratory syndrome coronavirus nonstructural protein 16 is necessary for interferon resistance and viral pathogenesis. *MSphere* **2**, 00346–00317 (2017).

74. J. Canton *et al.*, MERS-CoV 4b protein interferes with the NF-κB-dependent innate immune response during infection. *PLoS Pathog.* **14**, e1006838 (2018).
75. P. C. Woo, S. K. Lau, K. S. Li, A. K. Tsang, K. Y. Yuen, Genetic relatedness of the novel human group C betacoronavirus to Tylonycteris bat coronavirus HKU4 and Pipistrellus bat coronavirus HKU5. *Emerg. Microbes Infect.* **1**, e35 (2012).
76. V. M. Corman *et al.*, Rooting the phylogenetic tree of Middle East respiratory syndrome coronavirus by characterization of a conspecific virus from an African bat. *J. Virol.* **88**, 11297–11303 (2014).
77. L. Yang *et al.*, MERS-related betacoronavirus in *Vespertilio superans* bats, China. *Emerg. Infect. Dis.* **20**, 1260–1262 (2014).
78. S. K. P. Lau *et al.*, Receptor usage of a novel bat lineage C betacoronavirus reveals evolution of Middle East respiratory syndrome-related coronavirus spike proteins for human dipeptidyl peptidase 4 binding. *J. Infect. Dis.* **218**, 197–207 (2018).
79. C. M. Luo *et al.*, Discovery of novel bat coronaviruses in South China that use the same receptor as Middle East respiratory syndrome coronavirus. *J. Virol.* **92**, e00116-18 (2018).
80. N. Chen *et al.*, Two novel porcine epidemic diarrhea virus (PEDV) recombinants from a natural recombinant and distinct subtypes of PEDV variants. *Virus Res.* **242**, 90–95 (2017).
81. A. Moreno *et al.*, Detection and full genome characterization of two beta CoV viruses related to Middle East respiratory syndrome from bats in Italy. *Virol. J.* **14**, 239 (2017).
82. J. Y. Lee, S. Bae, J. Myoung, Middle East respiratory syndrome coronavirus-encoded accessory proteins impair MDA5-and TBK1-mediated activation of NF-κB. *J. Microbiol. Biotechnol.* **29**, 1316–1323 (2019).
83. J. Y. Lee, S. Bae, J. Myoung, Middle East respiratory syndrome coronavirus-encoded ORF8b strongly antagonizes IFN-β promoter activation: Its implication for vaccine design. *J. Microbiol.* **57**, 803–811 (2019).
84. K. Nakagawa, K. Narayanan, M. Wada, S. Makino, Inhibition of stress granule formation by Middle East respiratory syndrome coronavirus 4a accessory protein facilitates viral translation, leading to efficient virus replication. *J. Virol.* **92**, e00902–e00918 (2018).
85. D. Niemeyer *et al.*, Middle East respiratory syndrome coronavirus accessory protein 4a is a type I interferon antagonist. *J. Virol.* **87**, 12489–12495 (2013).
86. H. H. Rabouw *et al.*, Middle East respiratory coronavirus accessory protein 4a inhibits PKR-mediated antiviral stress responses. *PLoS Pathog.* **12**, e1005982 (2016).
87. K. L. Siu *et al.*, Middle east respiratory syndrome coronavirus 4a protein is a double-stranded RNA-binding protein that suppresses PACT-induced activation of RIG-I and MDA5 in the innate antiviral response. *J. Virol.* **88**, 4866–4876 (2014).
88. J. Ortego, J. E. Ceriani, C. Patiño, J. Plana, L. Enjuanes, Absence of E protein arrests transmissible gastroenteritis coronavirus maturation in the secretory pathway. *Virology* **368**, 296–308 (2007).
89. D. Schoeman, B. C. Fielding, Coronavirus envelope protein: Current knowledge. *Virol. J.* **16**, 69 (2019).
90. J. Gutiérrez-Álvarez *et al.*, Genetically engineered live-attenuated Middle East respiratory syndrome coronavirus viruses confer full protection against lethal infection. *MBio* **12**, e00103–e00121 (2021).
91. M. L. DeDiego *et al.*, A severe acute respiratory syndrome coronavirus that lacks the E gene is attenuated in vitro and in vivo. *J. Virol.* **81**, 1701–1713 (2007).
92. F. Fischer, C. F. Stegen, P. S. Masters, W. A. Samsonoff, Analysis of constructed E gene mutants of mouse hepatitis virus confirms a pivotal role for E protein in coronavirus assembly. *J. Virol.* **72**, 7885–7894 (1998).
93. J. L. Nieto-Torres, C. Verdiá-Báguena, C. Castaño-Rodriguez, V. M. Aguilella, L. Enjuanes, Relevance of viroporin ion channel activity on viral replication and pathogenesis. *Viruses* **7**, 3552–3573 (2015).
94. J. L. Nieto-Torres *et al.*, Severe acute respiratory syndrome coronavirus envelope protein ion channel activity promotes virus fitness and pathogenesis. *PLoS Pathog.* **10**, e1004077 (2014).
95. J. M. Jimenez-Guardeño *et al.*, The PDZ-binding motif of severe acute respiratory syndrome coronavirus envelope protein is a determinant of viral pathogenesis. *PLoS Pathog.* **10**, e1004320 (2014).
96. C. Castaño-Rodriguez *et al.*, Role of severe acute respiratory syndrome coronavirus viroporins E, 3a, and 8a in replication and pathogenesis. *MBio* **9**, e2325–e2317 (2018).
97. E. A. J. Alsaadi, B. W. Neuman, I. M. Jones, A fusion peptide in the spike protein of MERS coronavirus. *Viruses* **11**, 825 (2019).
98. Z. Qian, S. R. Dominguez, K. V. Holmes, Role of the spike glycoprotein of human Middle East respiratory syndrome coronavirus (MERS-CoV) in virus entry and syncytia formation. *PLoS One* **8**, e76469 (2013).
99. B. M. Waring *et al.*, MicroRNA-based attenuation of influenza virus across susceptible hosts. *J. Virol.* **92**, e01741–e01717 (2018).
100. L. Morales *et al.*, SARS-CoV-encoded small RNAs contribute to infection-associated lung pathology. *Cell Host Microbe* **21**, 344–355 (2017).
101. E. Petersen *et al.*, Comparing SARS-CoV-2 with SARS-CoV and influenza pandemics. *Lancet Infect. Dis.* **20**, e238–e244 (2020).
102. G. Hamilton, Virology: The gene weavers. *Nature* **441**, 683–685 (2006).
103. M. R. Denison, R. L. Graham, E. F. Donaldson, L. D. Eckerle, R. S. Baric, Coronaviruses: An RNA proofreading machine regulates replication fidelity and diversity. *RNA Biol.* **8**, 270–279 (2011).
104. L. Enjuanes, F. Almazán, I. Sola, S. Zuñiga, Biochemical aspects of coronavirus replication and virus-host interaction. *Annu. Rev. Microbiol.* **60**, 211–230 (2006).